Green Energy and Intelligent Transportation 1 (2022) 100025

Contents lists available at ScienceDirect

Green Energy and Intelligent Transportation

journal homepage: www.journals.elsevier.com/green-energy-and-intelligent-transportation

Full Length Article

Impact of battery cell imbalance on electric vehicle range☆

Jun Chen[a,*], Zhaodong Zhou[a], Ziwei Zhou[a], Xia Wang[b], Boryann Liaw[c]

[a] Department of Electrical and Computer Engineering, Oakland University, Rochester, MI 48309, USA
[b] Department of Mechanical Engineering, Oakland University, Rochester, MI 48309, USA
[c] Idaho National Laboratory, Idaho Falls, ID 83415, USA

HIGHLIGHTS

- A simulation model to assess electric vehicles range reduction due to cell-to-cell variation is constructed.
- A statistical analysis on electric vehicles range reduction for different variation configurations is performed.
- Nonlinear range reduction due to cell capacity variations is found.

GRAPHICAL ABSTRACT

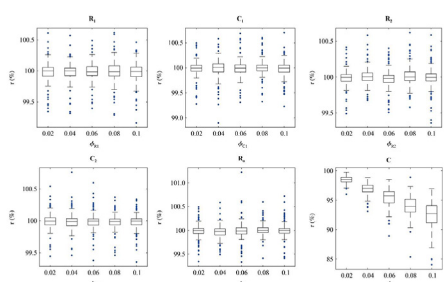

ARTICLE INFO

Keywords:
Electric vehicles
Battery range
Cell imbalance
Simulation

ABSTRACT

Due to manufacturing variation, battery cells often possess heterogeneous characteristics, leading to battery state-of-charge variation in real-time. Since the lowest cell state-of-charge determines the useful life of battery pack, such variation can negatively impact the battery performance and electric vehicles range. Existing research has been focused on control design to mitigate cell imbalance. However, it is yet unclear how much impacts the cell imbalance can have on electric vehicle range. This paper closes this knowledge gap by using a simulation environment consisting of real-world driving speed data, vehicle longitudinal control, propulsion and vehicle dynamics, and cell level battery modeling. In particular, each battery cell is modeled as an equivalent circuit model, and variations among cell parameters are introduced to assess their impact on electric vehicles range and to identify the most influential parameter variations. Simulation results and analysis can be used to assist balancing control design and to benchmark control performance.

☆ This work was supported in part by the faculty startup fund from School of Engineering and Computer Science at Oakland University and in part by Michigan Space Grant Consortium grant #80NSSC20M0124. BL would like to acknowledge that the authorship is voluntary on personal basis and that the statements and opinions in this article are solely those of the authors. Nothing in this article represents the work, views or positions of the Idaho National Laboratory (INL), the U.S. Department of Energy (DOE) or any of their customers. This manuscript has been authored by Battelle Energy Alliance, LLC under Contract No. DE-AC07-05ID14517 with the U.S. DOE. The publisher, by accepting the article for publication, acknowledges that the United States Government retains a nonexclusive, paid-up, irrevocable, worldwide license to publish or reproduce the published form of this manuscript, or allow others to do so, for United States Government purposes.

* Corresponding author.
E-mail address: junchen@oakland.edu (J. Chen).

https://doi.org/10.1016/j.geits.2022.100025
Received 8 July 2022; Received in revised form 13 August 2022; Accepted 16 August 2022
Available online 23 September 2022

1. Introduction

Electric vehicles (EVs), which are projected to make up 31% of the global fleet by 2050 [1], have been considered to be a promising way to combat climate change, reducing over 3000 kg carbon dioxide emission per vehicle per year [2]. In the meanwhile, highly efficient battery systems have been considered as key enablers to EVs and stationary smart grid applications [3–7]. EV battery pack usually consists of hundreds of cells, each of which can have different dynamic characteristics due to manufacturing and operation variations, leading to state-of-charge imbalance among battery cells [8–10]. Since the weakest cell limits the useable capacity of the whole battery pack, such state-of-charge imbalance would result in reduced EV range over single charge as well as life cycle, and can lead to safety issue such as thermal runaway [11–14]. To alleviate battery cell imbalance, active cell balancing control using a balancing circuit such as flyback DC/DC converter and half-bridge converter have been proposed in literature [12,15–17], which can be either *dissipative* or *nondissipative*. Correspondingly, various control methods have been proposed to conduct the active cell balancing control [15–20], ranging from rule-based control [21], simple feedback control [22], to advanced control like model predictive control (MPC) [13,23–25].

However, although the active battery balancing control has drawn extensive attentions and the aforementioned research demonstrate promising results on mitigating cell imbalance, it is yet unclear how the cell imbalance impacts EV range. In other words, a formal and numerical quantification on EV range reduction that is attributed to cell imbalance has not been reported in literature, and is much needed. Without this knowledge, most of existing research endeavors assume certain variations among all cell parameters [11,13,25], which can lead to unrealistic simulation assumption and increase control complexity unnecessarily. Furthermore, as there is no formal quantification on the range reduction due to cell imbalance, there is no benchmark to evaluate the control algorithms that aim at mitigating cell imbalance. Therefore, the performance of the aforementioned balancing controllers becomes obsolete.

To address this limitation, a simulation model is constructed that includes a speed controller to command battery power based on the actual and target vehicle speeds. Furthermore, battery cell dynamics are modeled using equivalent circuit model (ECM) with heterogeneous parameters. Finally, an EV propulsion model and a quarter car longitudinal model are used to simulate the vehicle behavior of a passenger EV car. Thorough analysis based on this simulation model are then conducted to understand the impact of battery cell imbalance on EV range. In particular, a total number of 125 trips are simulated based on real-world vehicle speed measurement data, which is available at National Renewable Energy Laboratory's Transportation Secure Data Center [26,27]. For each trip, different variation levels of cell parameters are introduced to calculate the corresponding range reduction. Statistical analysis is then performed to identify the impact of each parameter variation on the EV range. Such analysis can be beneficial for the control design and benchmarking. For example, several parameters are found to have no statistical influence on average EV range, and therefore it is not necessary for balancing control algorithm to explicitly estimate those parameters. Compared to relevant literature on battery inconsistency, such as modeling, estimation, and diagnosis [28–32], our work is different as we focus on evaluating the impact of battery cell variations in the context of EV ranges. As a full EV propulsion system is modeled and utilized, the propagation of the impact of cell level variation is explicitly evaluated and quantified.

The rest of this paper is organized as follows. Section 2 discusses the equivalent circuit model for each cell and the whole battery pack, while Section 3 presents the problem formulation with the main research question. Section 4 provides details on the simulation model used for numerical studies, and Section 5 presents simulation results and discusses the main findings. The paper is concluded in Section 6.

2. Battery dynamics

The dynamic of a battery cell can be modeled as an equivalent circuit model (ECM) [33–38], as shown in Fig. 1, where V_{oc} is the open circuit voltage, v is the terminal voltage, and i is current drawn from the cell with the convention that positive value of i indicates discharging from the cell and negative value indicates charging. Denote s as the cell SOC, V_1 and V_2 as the relaxation voltages over the two capacitors capturing fast and slow dynamics respectively. The dynamics of ECM are then specified by Ref. [38].

$$\dot{s} = -\eta \frac{i}{3600 \times C} \tag{1a}$$

$$\dot{V}_1 = -\frac{V_1}{R_1 C_1} + \frac{i}{C_1} \tag{1b}$$

$$\dot{V}_2 = -\frac{V_2}{R_2 C_2} + \frac{i}{C_2} \tag{1c}$$

$$\dot{T}_c = \frac{Q}{C_{p,c}} + \frac{T_s - T_c}{R_c C_{p,c}} \tag{1d}$$

$$\dot{T}_s = \frac{T_c - T_s}{R_c C_{p,s}} + \frac{T_f - T_s}{R_u C_{p,s}} \tag{1e}$$

$$y = V_{oc} - V_1 - V_2 - iR_o. \tag{1f}$$

Note that in (1), η is the coulombic efficiency, C is the cell capacity with unit of Amp-Hour, T_c and T_s are the cell core and surface temperature respectively, T_f is the coolant flow temperature, Cp,c and Cp,s are heat capacities of the battery core and surface respectively, R_c is the conduction resistance between T_c and T_s while R_u is the convection resistance between T_f and T_s. Finally, Q is the heat generation defined by

$$Q = i(V_{oc} - y) - I\frac{T_s + T_c}{2}\frac{\mathrm{d}V_{oc}}{\mathrm{d}T}.$$

Note that V_{oc}, R_o, R_1, R_2, C_1 and C_2 are all dependent on SOC s and temperatures T_s and T_c, where this nonlinear dependency can be denoted as, for $\sigma = \{V_{oc}, R_o, R_1, R_1, C_1, C_2\}$,

$$\sigma = f_\sigma(s, T_c, T_s). \tag{2}$$

Therefore (1) is a nonlinear model. In this paper, we adopt the parameters in Ref. [38] for model (1)–(2) for a nominal battery cell.

Now consider an EV battery system as shown in Fig. 2, where N cells are connected in series to provide current I as requested by EV propulsion system. Due to cell variations, the SOC among cells can be significantly different, even if they are initialized all the same SOC level. To address this issue, a balancing controller can be used to draw current from cells with higher SOC to charge cells with lower SOC. Such

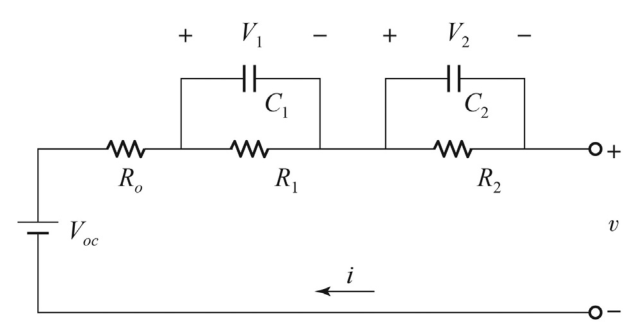

Fig. 1. Equivalent circuit model of a battery cell.

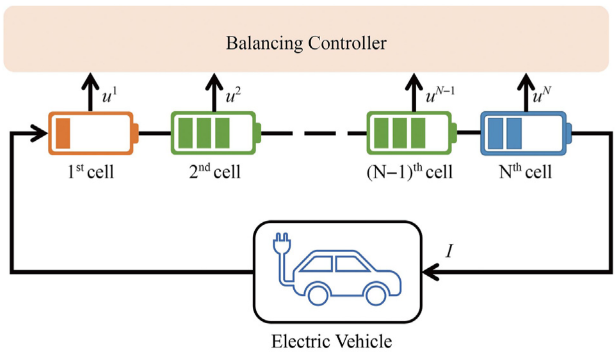

Fig. 2. Structure of series connected battery cell and balancing current [25].

balancing currents is denoted as u^n for the n^{th} cell. Denote cell current and terminal voltage for n^{th} cell as i^n and v^n, respectively, and denote the voltage and power of the battery pack as v_b and P_b, respectively. Then it is trivial to see that

$$i^n = I + u^n \tag{3a}$$

$$v_b = \sum\nolimits_{n=1}^{N} v^n \tag{3b}$$

$$P_b = Iv_b. \tag{3c}$$

3. Problem statement

Due to manufacturing variations and/or aging condition variations, the parameters for (1)–(2) can be significantly different for each cell. Particularly we consider variations of parameters R_o, R_1, R_2, C_1, C_2 and C. For n^{th} cell, we model the cell variation as follows. For each parameter $\sigma \in \{R_o, R_1, R_2, C_1, C_2, C\}$,

$$\sigma^n = \begin{cases} (1+\phi_\sigma^n) f_\sigma(s^n, T_c^n, T_f^n) & \text{if} \quad \sigma \in \{R_o, R_1, R_2, C_1, C_2\}, \\ (1+\phi_\sigma^n) C_0 & \text{if} \quad \sigma = C, \end{cases} \tag{4}$$

where C_0 and f_σ are the nominal values adopted from Ref. [38]. Now consider an EV battery system as shown in Fig. 2, where the parameter variations for each cell is modeled by (4). We define the variation level ϕ_σ for $\sigma \in \{R_o, R_1, R_2, C_1, C_2, C\}$ as the standard deviation of ϕ_σ^n, i.e.,

$$\phi_\sigma = \sqrt{\frac{1}{N}\sum\nolimits_{n=1}^{N} (\phi_\sigma^n - \mu_\sigma)^2}, \tag{5}$$

where μ_σ is the mean of ϕ_σ^n, i.e.,

$$\mu_\sigma = \frac{1}{N}\sum\nolimits_{n=1}^{N} \phi_\sigma^n. \tag{6}$$

Note that ϕ_σ^n in (4) is the deviation of parameters from their nominal values. Therefore, μ_σ denotes the mean of the parameters deviation from their nominal values.

The research question we intend to answer is, how much impacts the cell variations can have on EV range. Specifically.

1. Which parameter among R_o, R_1, R_2, C_1, C_2 and C has largest influence on EV range? and
2. How is the EV range impacted by the variation level ϕ_σ, $\sigma \in \{R_o, R_1, R_2, C_1, C_2, C\}$?

To answer these research questions, we conducted simulations using battery model (1), (2), (3) and (4), together with an EV model. In the next section, we will introduce the simulation environment in greater details.

4. Simulation model

Diagram of the simulation model is shown in Fig. 3. In particular, a reference speed profile v_{ref} is used as input to a speed controller, which requests a battery power P_b^r from the battery pack. Upon receiving this command, the battery management system (BMS) calculates, based on the latest battery and cell states, the pack current I and balancing current u^n for $n = 1, \ldots, N$. The battery dynamic model simulates (1)–(4) and then outputs the actual battery power P_b to drive the vehicle.

Note that in Fig. 3, all control algorithm blocks are marked in light blue while physical dynamic blocks are marked in light orange. In the rest of this session, we discuss the reference speed profile, speed controller, and propulsion & vehicle dynamics blocks in more details.

4.1. Reference speed data

Vehicle speed dataset[1] provided by The Transportation Secure Data Center (TSDC) at National Renewable Energy Laboratory [26,27] was used to generate reference speed data for simulation purpose. The dataset includes global positioning system (GPS) readings and the length of trip varies from several minutes to hours. To have longer trips for simulation purpose, short trips are concatenated together to create longer trip so that the travel distance of each trip is longer than the range of EV on a single charge.

In this work, a total number of 125 trips are generated. Snapshots of 1 h of speed reference data are shown in Fig. 4 for Dataset #5 (top of Fig. 4) and #6 (bottom of Fig. 4), showing that both dynamic and steady state maneuvers are present in the dataset. Note that Dataset #5 and #6 are randomly selected for illustrative purpose. Top half of Fig. 5 plots the average trip speed for each dataset, where the average speed varies from slow (around 50 km/h) to extremely fast (around 150 km/h). Note that the bottom half of Fig. 5 will be discussed shortly in Section 5.

4.2. Speed controller

A PI speed controller is utilized to track the reference speed, i.e.,

$$e_v(t) = v_{ref}(t) - v_x(t) \tag{7a}$$

$$P_b^r(t) = K_p e_v(t) + K_i \int_0^t e_v(\tau)\mathrm{d}\tau, \tag{7b}$$

where $e_v(t)$ is the instantaneous speed tracking error. The output of this speed controller is the requested power P_b^r, which is then fed into BMS and battery dynamic model (1)–(4) to produce actual battery power. To reduce the influence of speed controller, the control gains are fixed for all simulations. Table 1 includes controller gain for PI controller (7), and snapshots of 1 h of requested battery power are shown in Fig. 6 for Dataset #5 (Top) and #6 (Bottom), corresponding to the reference speed shown in Fig. 4.

4.3. Propulsion and vehicle dynamics

To reduce simulation time, a quarter car model is used to simulate the vehicle dynamic. As lateral dynamic is not considered in this study, a quarter car model is found to be sufficient to evaluate EV energy consumption [39]. This section briefly introduces the model, and more details can be found in Refs. [39–41]. The longitudinal dynamics of a quarter car model can be represented as follow,

$$\dot{v}_x = \frac{n_w}{m}F_x - g\sin\sigma_b - \frac{1}{m}F_a \tag{8a}$$

[1] Available at: https://www.nrel.gov/transportation/securetransportation-data/. Accessed Sep. 15, 2021.

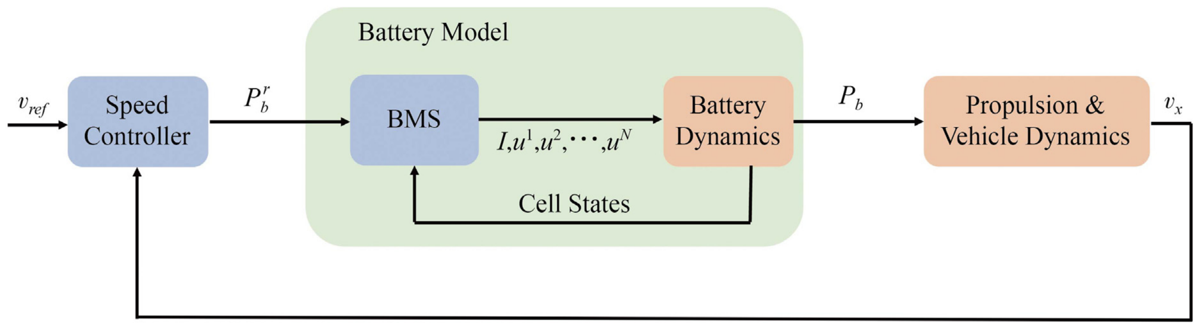

Fig. 3. Diagram of the simulation model.

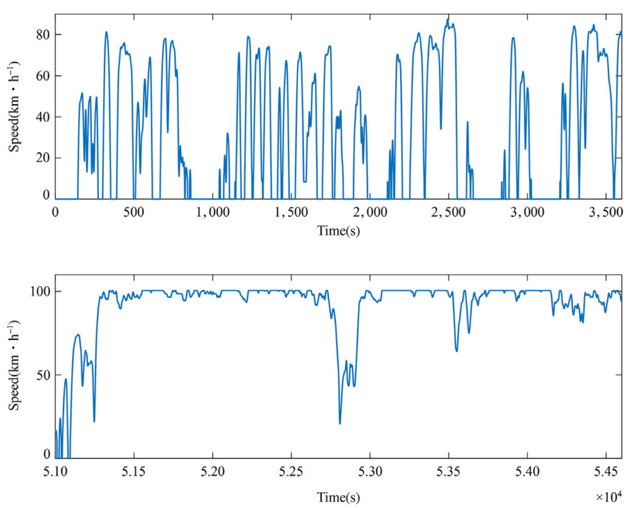

Fig. 4. Snapshot of the reference speed data from Dataset #5 (top) and #6 (bottom).

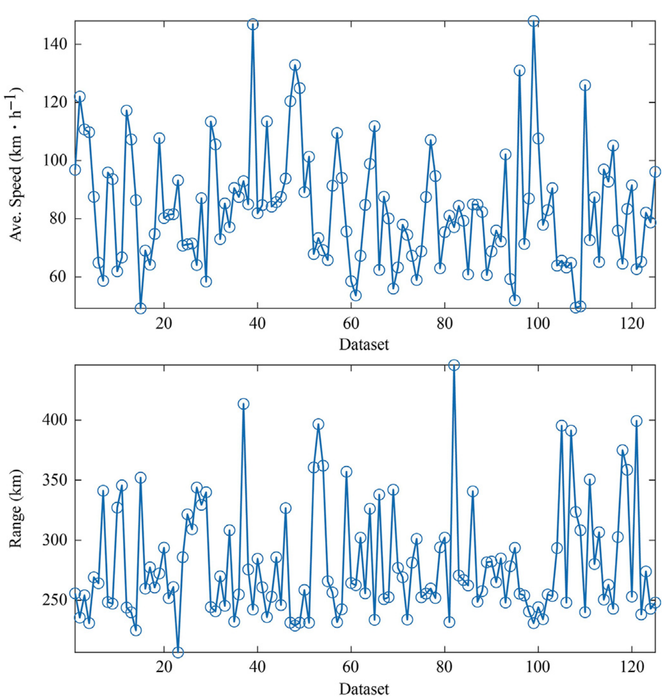

Fig. 5. Average trip speed (top) and total EV range (bottom) for each dataset when all cells are identical (i.e., 0 variation level for all parameters).

$$\dot{\omega} = \frac{1}{I_w}\left(\frac{T}{n_w} - F_x R\right), \tag{8b}$$

where m is the mass of the vehicle, n_w is the number of driving wheels, which equals 2 for front/rear driving vehicle and 4 for all wheel drive configuration, σ_b is the road bank angle, I_w is the wheel rotational inertial, T is the total driving torque (as applied to all driving wheels) and F_x is the total tire force, as computed by the following Magic formula [42].

$$F_x = F_z D \sin\{C \arctan[Bs_r - E(Bs_r - \arctan(Bx))]\}, \tag{9}$$

with the parameters B, C, D, E given as 10, 1.9, 1 and 0.97. Note that F_z is normal force and s_r is slip ratio defined as

Table 1
Parameters for the simulation models. Partiallydopted from Ref. [39].

Parameter [Unit]	Physical Meaning	Value
m[kg]	Car mass	1500
n_w [−]	# of driving wheel	2
R[m]	Effective wheel radius	0.2159
σ_b	Bank angle	0
ρ[kg/m^3]	Air density	1.225
C_d [−]	Air drag coefficient	0.389
A_F	Front area	2
η_D[%]	Propulsion efficiency	100
T_d[ms]	Propulsion time constant	300
K_p [−]	Proportion gain	50
K_i [−]	Integral gain	300

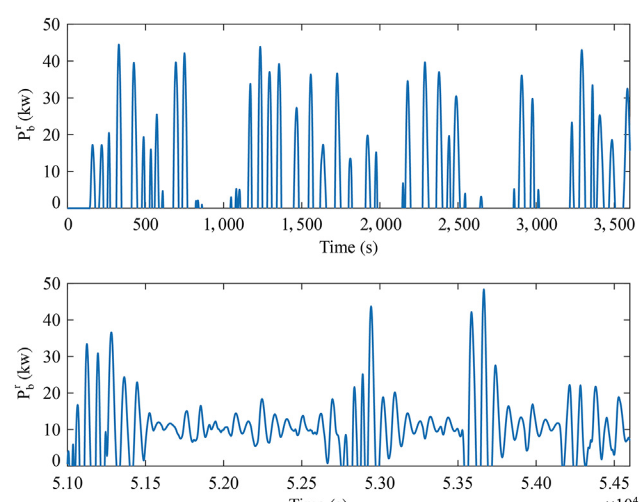

Fig. 6. Snapshot of the requested power for Dataset #5 (Top) and #6 (Bottom), corresponding to the reference speed shown in Fig. 4.

$$s_r = \frac{\omega R - v_x}{v_x}, \tag{10}$$

with R being the wheel effective radius.

Finally, according to Ref. [40], the aerodynamic drag force F_a in (9) can be modeled by (assuming wind speed is 0):

$$F_a = \frac{1}{2}\rho C_d A_F v_x^2, \tag{11}$$

where ρ is the air mass density, C_d is the aerodynamic drag coefficient, A_F is the effective front area.

Table 2
EV mileage with identical battery cells.

Dataset #	1	2	3	4	5	6	7	8	9	10
Range [km]	255.779	235.578	254.18	230.965	269.174	264.181	341.252	248.474	247.146	327.22
Dataset #	11	12	13	14	15	16	17	18	19	20
Range [km]	345.675	243.91	239.922	224.956	352.101	259.714	277.437	260.626	272.358	293.817
Dataset #	21	22	23	24	25	26	27	28	29	30
Range [km]	251.793	261.05	206.57	285.894	321.649	309.173	343.951	329.553	340.009	244.328
Dataset #	31	32	33	34	35	36	37	38	39	40
Range [km]	240.794	269.979	245.388	308.388	232.254	254.82	413.544	275.641	242.289	284.615
Dataset #	41	42	43	44	45	46	47	48	49	50
Range [km]	260.849	235.987	252.991	285.85	245.982	326.779	231.37	228.897	231.36	258.609
Dataset #	51	52	53	54	55	56	57	58	59	60
Range [km]	231.291	360.541	396.609	362.02	265.874	256.521	231.76	242.509	357.009	264.379
Dataset #	61	62	63	64	65	66	67	68	69	70
Range [km]	262.585	302.167	255.735	326.335	233.714	338.026	250.941	252.596	342.117	277.04
Dataset #	71	72	73	74	75	76	77	78	79	80
Range [km]	269.195	233.934	281.388	301.175	252.483	255.535	259.798	251.881	294.1	302.19
Dataset #	81	82	83	84	85	86	87	88	89	90
Range [km]	231.779	445.843	270.621	266.908	262.342	340.762	248.765	257.622	281.693	282.283
Dataset #	91	92	93	94	95	96	97	98	99	100
Range [km]	265.028	284.842	248.087	278.365	293.719	255.467	254.011	240.684	230.937	244.27
Dataset #	101	102	103	104	105	106	107	108	109	110
Range [km]	234.187	254.8	253.562	293.461	395.408	248.1	391.27	323.578	308.322	240.079
Dataset #	111	112	113	114	115	116	117	118	119	120
Range [km]	350.525	280.213	306.69	250.522	262.86	242.944	302.686	374.982	358.618	253.068
Dataset #	121	122	123	124	125	–	–	–	–	–
Range [km]	399.29	238.187	273.975	242.9	248.115	–	–	–	–	–

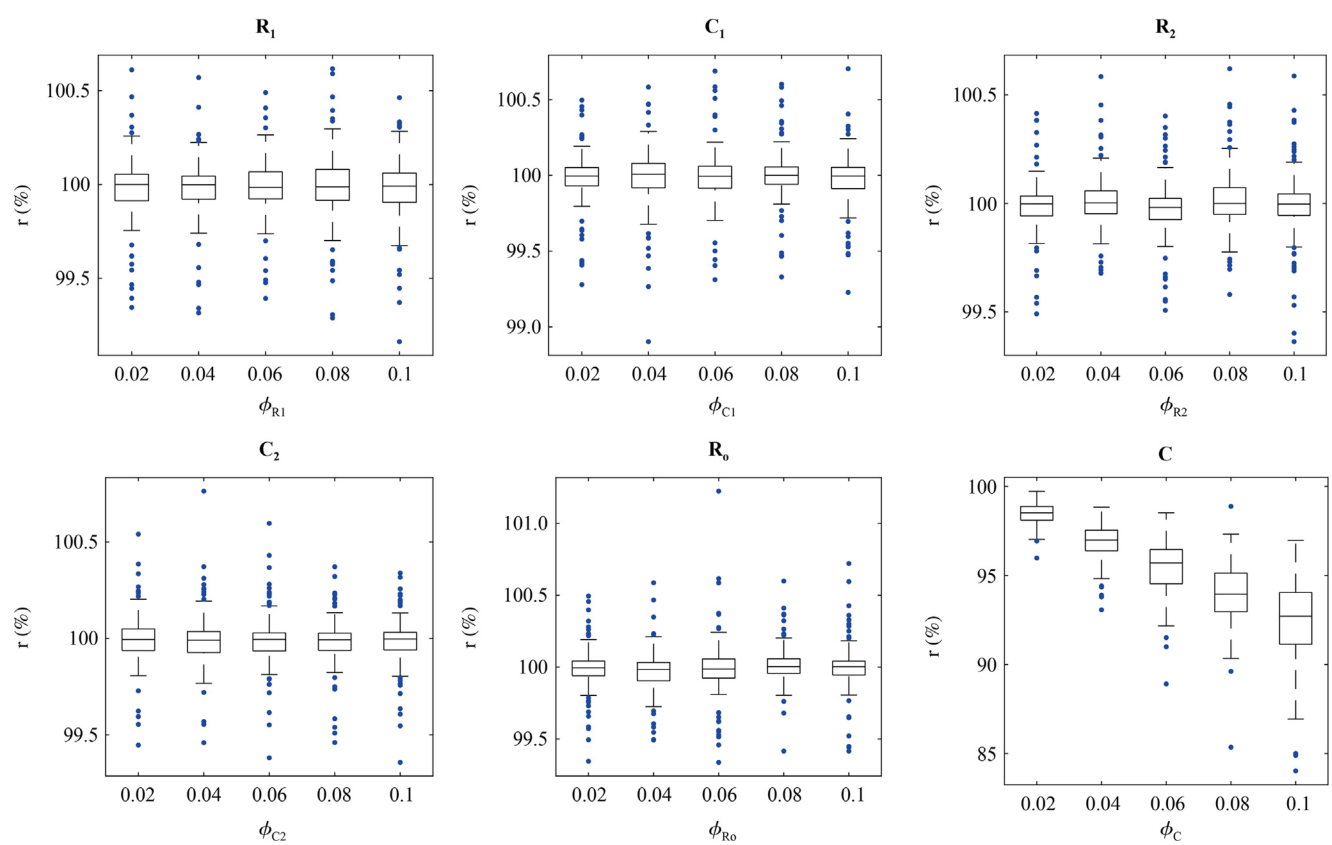

Fig. 7. Range variation with respect to cell variation level.

The propulsion dynamic (electric motor, transmission, and final drive) is modeled as a first order transfer function, as follows,

$$G(s) = \frac{P_w}{P_b} = \frac{\eta_D}{T_d s + 1} \tag{12}$$

where P_b is the actual battery power and P_w is the actual power delivered at the wheel, η_D is the overall propulsion efficiency, and T_d represents the time constant of the entire propulsion system. Finally, the power P_w and driving wheel torque T at the wheel satisfy

$$P = T\omega. \tag{13}$$

Table 1 lists all the parameters for the propulsion and vehicle dynamic models used in this study.

5. Numerical analysis

5.1. Nominal simulation

As benchmarking, we first run the simulation without any cell variation. In other words, 10 identical cells are used to simulate the battery pack, i.e., $N = 10$ and $\mu_\sigma = \phi_\sigma = 0$ for all $\sigma \in \{R_o, R_1, R_2, C_1, C_2, C\}$. Note that $N = 10$ is selected to reduce simulation time. The output battery power from 10 cells is then scaled to meet the power request of a full size EV. In this case, the EV range for each trip is documented in Table 2 and plotted in the bottom half of Fig. 5. As can be seen, the nominal range varies from around 200 km to around 450 km, due to the impact of driving maneuvers. Such variation is a result of the wide spread of driving maneuvers included in the dataset and justifies the use of the selected dataset since it exposes the simulation to a variety of scenarios.

5.2. Impacts of cell variations

To evaluate the impact of cell variations (i.e., research question 1 and 2 above), simulations are conducted over several variation configurations. For each configuration, one (and only one) parameter $\sigma \in \{R_o, R_1, R_2, C_1, C_2, C\}$ is selected to vary with normal distribution such that $\mu_\sigma = 0$ and $\phi_\sigma > 0$, while the other parameters σ' are assumed to have 0 variation level (i.e., $\mu_{\sigma'} = \phi_{\sigma'} = 0$). With a slight abuse of notation, we use $\phi_\sigma(x)$, where $\sigma \in \{R_o, R_1, R_2, C_1, C_2, C\}$ and $x \in \{0.02, 0.04, 0.06, 0.08, 0.1\}$, to denote the variation configuration where σ is selected to have a variation level $\phi_\sigma = x$. Therefore, there are a total number of 30 variation configurations (6 parameters, and 5 variation levels for each parameter). Moreover, cell balancing control is assumed to be absent in this study. In other words, the BMS in Fig. 3 only calculates pack current I and set u^1, …, u^n all to 0. Note that similar to the nominal simulation, $N = 10$ is used to reduce simulation time. The battery output power is then scaled to meet the power request of a full size EV.

For each variation configuration $\phi_\sigma(x)$, all 125 trips are simulated. For k^{th} trip, denote the EV range at nominal condition (i.e., when $\phi_\sigma = 0$ for all σ) as $m^k[0]$, and denote the EV range for variation configuration $\phi_\sigma(x)$ as $m^k[\phi_\sigma(x)]$. Then the range ratio on the k^{th} trip can then be calculated as the ratio between $m^k[0]$ and $m^k[\phi_\sigma(x)]$, as follows.

$$r^k[\phi_\sigma(x)] = \frac{m^k[\phi_\sigma(x)]}{m^k[0]} \times 100\%. \tag{14}$$

Note that here $r^k[\phi_\sigma(x)]$ quantifies the impact of the variation $\phi_\sigma(x)$ on the EV range on k^{th} trip. When $r^k[\phi_\sigma(x)] > 100\%$, the cell imbalance would increase the EV range and on the other hand, when $r^k[\phi_\sigma(x)] < 100\%$, the cell imbalance negatively impact the EV range by reducing it.

Table 3
EV Mileage Ratio For $\varphi_C = 0.02$ and $\varphi_C = 0.1$

Dataset #	1	2	3	4	5	6	7	8	9	10
$r[\varphi_C(0.02)]$	98.87%	98.42%	98.32%	98.09%	98.82%	96.95%	99.48%	98.69%	97.82%	97.82%
$r[\varphi_C(0.1)]$	91.25%	94.08%	90.53%	89.74%	95.24%	91.49%	93.15%	90.17%	90.99%	85.01%
Dataset #	11	12	13	14	15	16	17	18	19	20
$r[\varphi_C(0.02)]$	98.57%	97.58%	97.69%	98.98%	98.68%	98.85%	98.05%	98.42%	98.68%	98.55%
$r[\varphi_C(0.1)]$	94.02%	93.82%	93.08%	92.42%	92.97%	92.44%	89.81%	92.77%	92.96%	94.04%
Dataset #	21	22	23	24	25	26	27	28	29	30
$r[\varphi_C(0.02)]$	98.32%	98.01%	99.06%	97.69%	99.61%	98.69%	97.88%	99.43%	99.18%	97.83%
$r[\varphi_C(0.1)]$	91.51%	94.09%	93.24%	88.52%	93.02%	90.77%	94.91%	92.23%	88.12%	94.48%
Dataset #	31	32	33	34	35	36	37	38	39	40
$r[\varphi_C(0.02)]$	98.86%	99.28%	98.50%	99.19%	98.05%	98.97%	99.55%	97.27%	98.12%	97.03%
$r[\varphi_C(0.1)]$	93.74%	91.19%	92.63%	95.79%	93.82%	90.87%	91.21%	84.89%	93.39%	92.04%
Dataset #	41	42	43	44	45	46	47	48	49	50
$r[\varphi_C(0.02)]$	98.95%	99.20%	97.54%	98.32%	98.33%	99.73%	98.40%	99.72%	98.09%	98.89%
$r[\varphi_C(0.1)]$	92.94%	92.37%	90.28%	91.76%	92.33%	93.89%	94.73%	92.41%	93.68%	92.13%
Dataset #	51	52	53	54	55	56	57	58	59	60
$r[\varphi_C(0.02)]$	98.69%	98.19%	99.10%	95.98%	97.40%	98.82%	98.51%	97.83%	99.21%	98.67%
$r[\varphi_C(0.1)]$	92.07%	92.72%	94.55%	84.03%	93.07%	88.43%	87.81%	91.12%	96.29%	91.52%
Dataset #	61	62	63	64	65	66	67	68	69	70
$r[\varphi_C(0.02)]$	99.37%	98.43%	98.47%	99.19%	98.07%	99.14%	97.68%	98.74%	98.47%	98.80%
$r[\varphi_C(0.1)]$	95.99%	96.24%	96.97%	95.33%	89.79%	93.74%	90.59%	92.14%	94.12%	96.10%
Dataset #	71	72	73	74	75	76	77	78	79	80
$r[\varphi_C(0.02)]$	98.45%	98.77%	98.63%	98.11%	98.77%	98.51%	98.42%	98.46%	98.81%	98.92%
$r[\varphi_C(0.1)]$	90.88%	94.17%	94.92%	92.38%	90.52%	93.78%	93.98%	91.99%	91.21%	94.15%
Dataset #	81	82	83	84	85	86	87	88	89	90
$r[\varphi_C(0.02)]$	98.05%	98.32%	98.39%	98.16%	98.56%	99.37%	98.65%	98.04%	98.39%	98.30%
$r[\varphi_C(0.1)]$	88.65%	93.80%	93.47%	91.14%	92.06%	94.33%	90.99%	89.44%	92.36%	95.35%
Dataset #	91	92	93	94	95	96	97	98	99	100
$r[\varphi_C(0.02)]$	99.07%	97.62%	98.28%	99.35%	98.68%	98.33%	99.34%	99.19%	99.08%	98.22%
$r[\varphi_C(0.1)]$	93.33%	90.44%	93.12%	92.87%	92.09%	94.86%	93.42%	90.91%	93.96%	92.06%
Dataset #	101	102	103	104	105	106	107	108	109	110
$r[\varphi_C(0.02)]$	97.72%	97.69%	98.48%	98.67%	98.70%	97.85%	98.43%	99.11%	98.25%	98.90%
$r[\varphi_C(0.1)]$	94.06%	90.76%	93.96%	92.79%	95.02%	89.57%	94.22%	94.44%	92.05%	93.17%
Dataset #	111	112	113	114	115	116	117	118	119	120
$r[\varphi_C(0.02)]$	98.57%	98.67%	98.86%	96.93%	97.58%	98.24%	98.76%	98.85%	99.42%	98.63%
$r[\varphi_C(0.1)]$	95.27%	93.21%	95.34%	86.94%	92.33%	96.95%	94.74%	92.59%	95.60%	90.63%
Dataset #	121	122	123	124	125	–	–	–	–	–
$r[\varphi_C(0.02)]$	99.01%	97.30%	98.57%	98.21%	97.97%	–	–	–	–	–
$r[\varphi_C(0.1)]$	96.15%	89.51%	92.59%	92.36%	88.74%	–	–	–	–	–

Fig. 7 plots the distribution (as box plot) of range ratio $\{r^k, k = 1, 2, \ldots, 125\}$ for each variation configuration. It can be seen that, while the range of individual trip is impacted by variations among R_o, C_1, R_1, C_2, and R_2, the average ratio remains 100%, indicating the average EV range seems not to be impacted by these parameter variations. On the other hand, the variation in cell capacity C seems to have the largest influence on EV range. Specifically, for $\phi_C(0.02)$ configuration, the average range ratio is 98.48%, while this ratio drops to 92.47% for $\phi_C(0.1)$. Moreover, for all ϕ_C configurations, all trips have a reduced range as $r^k < 100\%$ for all $\phi_C(x)$, $x \in \{0.02, 0.04, 0.06, 0.08, 0.1\}$. Finally, details on each trip range ratio for variation levels of 0.02 and 0.1 for cell capacity C are documented in Table 3 and plotted in Fig. 8.

To understand how the variation level ϕ_C impacts the EV range, Fig. 9 plots the average range ratio as with respect to ϕ_C, together with a 3rd order polynomial fit. Note that the 3rd fit has an average error of 0.1264%, indicating that the impact of ϕ_C on EV range is nonlinear.

5.3. Discussion

Based on Fig. 7, it is clear that the variations on R_1, C_1, R_2, C_2 and R_o do not impact EV range, though for each trip there can be up to $\pm 0.5\%$ range difference due to different dynamic behavior. This aligns with intuition behind ECM, in which C_1 and C_2 only impacts the cell transient behavior and do not influence its steady state behavior. Furthermore, the capacitors, as used in ECM, are assumed to have zero energy loss. On the other hand, though the variations of R_1, R_2, and R_o do change the DC resistance of each individual cell, the overall DC resistance of the battery pack is not impacted, since $\mu_\sigma = 0$ for $\sigma \in \{R_1, R_2, R_o\}$.

Moreover, according to Fig. 7, it is evident that the variation of cell capacity C has the largest influence on EV range. This is also reasonable considering that we only simulate series connection, and the overall Amp-Hour capacity of a series string is mainly determined by the lowest cell capacity.

The results presented here can be very helpful for control design. Note that in literature [11,13,25], active balancing control has been designed and evaluated by assuming all cell parameters are heterogeneous, which can unnecessarily increase control complexity. According to results presented here, only cell capacity variation needs to be incorporated into control design. Furthermore, since all the other parameters do not impact EV range in statistical sense, there is no need to online estimate their variation level, hence reducing the control complexity even further.

Finally, as described by (1), cell temperatures are considered as states of cells, as opposed to parameters. Therefore, their variations are not treated in the same way as cell parameters. In fact, when cell parameters variation level change, the evolution of temperature is different as well. Therefore, the variation of temperature, which comes from the change of model parameters, does impact the EV range variations. In the future, we would also investigate the impact of environment temperature on EV range variation.

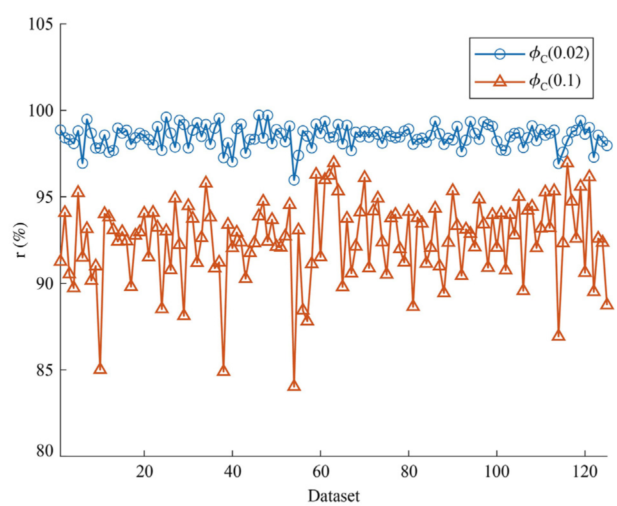

Fig. 8. Range ratio for variation levels of 0.02 and 0.1 for cell capacity C.

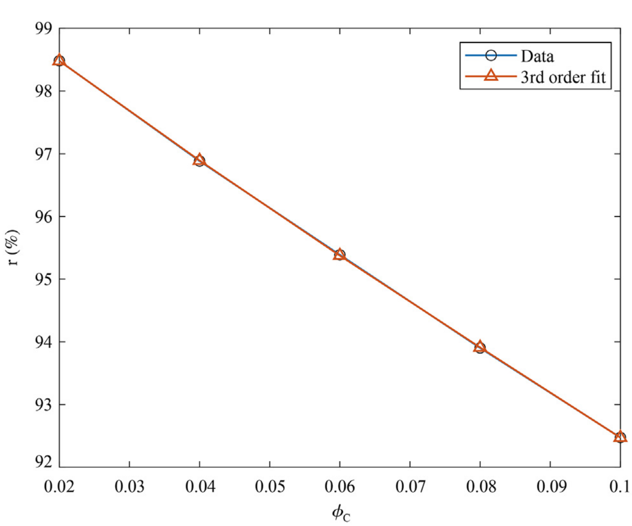

Fig. 9. Range ratio w.r.t. variation level of cell capacity C, i.e., $r[\varphi_C]$, and a 3rd polynomial fit.

6. Conclusion

This paper focuses on investigating the battery cell imbalance and its impact on electric vehicles range. Existing work has been mainly focused on control design to mitigate the impact of cell imbalance, yet a formal quantification of this impact is missing. To address this issue, we construct a simulation environment that utilizes real-world driving speed data, an electric vehicles propulsion model, a longitudinal vehicle dynamic model, and equivalent circuit models for battery cell and pack dynamics. Simulation results suggest that for most parameters, their zero-mean variations do not impact the overall electric vehicles range, and the most influence factor is cell capacity, which can lead to nonlinear range reduction. Future work include (1) incorporating prior control design [25] into the developed simulation framework, (2) improving the model predictive control of [25] by online estimating the variation level of cell capacity, and (3) benchmarking the balancing control performance by investigating impulsive control strategy, representative driving cycle generation [43], and collaborative control with other energy entities [44,45].

Declaration of Competing Interest

The authors declare the following:

All authors have participated in (a) conception and design, or analysis and interpretation of the data; (b) drafting the article or revising it critically for important intellectual content; and (c) approval of the final version.
This manuscript has not been submitted to, nor is under review at, another journal or other publishing venue.
The authors have no affiliation with any organization with a direct or indirect financial interest in the subject matter discussed in the manuscript.

References

[1] Electric vehicles projected to make up 31% of the global fleet by 2050, URL: https://electrek.co/2021/10/26/electric-vehicles-projected-to-make-up-31-of-the-global-fleet-by-2050/, accessed on July 16, 2022.

[2] Department of Energy, Emissions from electric vehicles, alternative fuels data center. Accessed on July 16, 2022.
[3] Kauer M, Narayanaswamy S, Steinhorst S, Lukasiewycz M, Chakraborty S. Many-to-many active cell balancing strategy design. In: The 20th asia and south pacific design automation conference. Chiba, Japan; 2015. p. 267–72.
[4] Chen J, Li Z, Yin X. Optimization of energy storage size and operation for renewable-ev hybrid energy systems. In: IEEE green technologies conference, denver, CO; 2021. April 7–9, 2021.
[5] Chen J, Garcia HE. Economic optimization of operations for hybrid energy systems under variable markets. Appl Energy 2016;177:11–24.
[6] Sepasi S, Ghorbani R, Liaw BY. A novel on-board state-of-charge estimation method for aged li-ion batteries based on model adaptive extended kalman filter. J Power Sources 2014;245:337–44.
[7] Chen J, Garcia HE. Operations optimization of hybrid energy systems under variable markets. In: 2016 American control conference (ACC), bosston, MA; July 6–8, 2016. p. 3212–8.
[8] Dubarry M, Vuillaume N, Liaw BY. Origins and accommodation of cell variations in li-ion battery pack modeling. Int J Energy Res 2010;34:216–31.
[9] Dubarry M, Vuillaume N, Liaw BY. From single cell model to battery pack simulation for li-ion batteries. J Power Sources 2009;186:500–7.
[10] Dubarry M, Devie A, Liaw BY. Cell-balancing currents in parallel strings of a battery system. J Power Sources 2016;321:36–46.
[11] Hoekstra F, Bergveld HJ, Donkers M. Range maximisation of electric vehicles through active cell balancing using reachability analysis. In: 2019 American control conference. Philadelphia, PA: ACC); July . p. 1567–72.
[12] Einhorn M, Roessler W, Fleig J. Improved performance of serially connected li-ion batteries with active cell balancing in electric vehicles. IEEE Trans Veh Technol 2011;60:2448–57.
[13] Hoekstra FS, Ribelles LW, Bergveld HJ, Donkers M. Real-time range maximisation of electric vehicles through active cell balancing using model-predictive control. In: 2020 American control conference, denver, CO; July 1–3, 2020. p. 2219–24.
[14] Smith K, Wood E, Santhanagopalan S, Kim G, Pesaran A. Advanced models and controls for prediction and extension of battery lifetime (presentation). 2014.
[15] Shang Y, Xia B, Zhang C, Cui N, Yang J, Mi CC. An automatic equalizer based on forward–flyback converter for series-connected battery strings. IEEE Trans Ind Electron 2017;64:5380–91.
[16] Shang Y, Cui N, Zhang C. An optimized any-cell-to-any-cell equalizer based on coupled half-bridge converters for series-connected battery strings. IEEE Trans Power Electron 2018;34:8831–41.
[17] Pinto C, Barreras JV, Schaltz E, Araujo RE. Evaluation of advanced control for li-ion battery balancing systems using convex optimization. IEEE Trans Sustain Energy 2016;7:1703–17.
[18] Narayanaswamy S, Park S, Steinhorst S, Chakraborty S. Multi-pattern active cell balancing architecture and equalization strategy for battery packs. In: Proc. Of the international symposium on low power electronics and design, seattle, WA; July 23–25, 2018. p. 1–6.
[19] Gao Z, Chin C, Toh W, Chiew J, Jia J. State-of-charge estimation and active cell pack balancing design of lithium battery power system for smart electric vehicle. J Adv Transport 2017:2017.
[20] Preindl M. A battery balancing auxiliary power module with predictive control for electrified transportation. IEEE Trans Ind Electron 2017;65:6552–9.
[21] Xu J, Cao B, Li S, Wang B, Ning B. A hybrid criterion based balancing strategy for battery energy storage systems. Energy Proc 2016;103:225–30.
[22] Wang C, Yin G, Lin F, Polis MP, Zhang C, Jiang J, et al. Balanced control strategies for interconnected heterogeneous battery systems. IEEE Trans Sustain Energy 2015; 7:189–99.
[23] Liu J, Chen Y, Fathy HK. Nonlinear model-predictive optimal control of an active cell-to-cell lithium-ion battery pack balancing circuit. IFAC-PapersOnLine 2017;50: 14483–8.
[24] McCurlie L, Preindl M, Emadi A. Fast model predictive control for redistributive lithium-ion battery balancing. IEEE Trans Ind Electron 2016;64:1350–7.
[25] Chen J, Behal A, Li C. Active cell balancing by model predictive control for real time range extension. In: 2021 IEEE conference on decision and control, austin, TX, USA; 2021.
[26] Fish J, Gonder J, Garikapati V, Cappellucci J, Borlaug B, Holden J, Boyce L. Transportation secure data center, technical report, DOE open energy data initiative (OEDI). National Renewable Energy Laboratory; 2015. URL: https://www.nrel.gov/transportation/secure-transportation-data/tsdc-drive-cycle-data.html.
[27] Gonder J, Burton E, Murakami E. Archiving data from new survey technologies: enabling research with high-precision data while preserving participant privacy. Transport Res Procedia 2015;11:85–97.
[28] Duan B, Li Z, Gu P, Zhou Z, Zhang C. Evaluation of battery inconsistency based on information entropy. J Energy Storage 2018;16:160–6.
[29] Hua Y, Zhou S, Cui H, Liu X, Zhang C, Xu X, Ling H, Yang S. A comprehensive review on inconsistency and equalization technology of lithium-ion battery for electric vehicles. Int J Energy Res 2020;44:11059–87.
[30] Feng F, Hu X, Hu L, Hu F, Li Y, Zhang L. Propagation mechanisms and diagnosis of parameter inconsistency within li-ion battery packs. Renew Sustain Energy Rev 2019;112:102–13.
[31] Yang C, Wang X, Fang Q, Dai H, Cao Y, Wei X. An online soc and capacity estimation method for aged lithium-ion battery pack considering cell inconsistency. J Energy Storage 2020;29:101250.
[32] Fan X, Zhang W, Wang Z, An F, Li H, Jiang J. Simplified battery pack modeling considering inconsistency and evolution of current distribution. IEEE Trans Intell Transport Syst 2020;22:630–9.
[33] Pei Z, Zhao X, Yuan H, Peng Z, Wu L. An equivalent circuit model for lithium battery of electric vehicle considering self-healing characteristic. J Control Sci Eng 2018;2018.
[34] Madani SS, Schaltz E, Knudsen Kær S. An electrical equivalent circuit model of a lithium titanate oxide battery. Batteries 2019;5:31.
[35] Liaw BY, Nagasubramanian G, Jungst RG, Doughty DH. Modeling of lithium ion cells—a simple equivalent-circuit model approach. Solid State Ionics 2004;175: 835–9.
[36] He H, Xiong R, Zhang X, Sun F, Fan J. State-of-charge estimation of the lithium-ion battery using an adaptive extended kalman filter based on an improved thevenin model. IEEE Trans Veh Technol 2011;60:1461–9.
[37] Wehbe J, Karami N. Battery equivalent circuits and brief summary of components value determination of lithium ion: a review. In: 2015 third international conference on technological advances in electrical, electronics and computer engineering. Beirut, Lebanon: TAEECE); 2015. p. 45–9.
[38] Lin X, Perez HE, Mohan S, Siegel JB, Stefanopoulou AG, Ding Y, Castanier MP. A lumped-parameter electro-thermal model for cylindrical batteries. J Power Sources 2014;257:1–11.
[39] J. Chen, M. Liang, X. Ma, Probabilistic analysis of electric vehicle energy consumption using MPC speed control and nonlinear battery model, in: 2021 IEEE green technologies conference, denver, CO, April 7–9, 2021..
[40] Rajamani R. Vehicle dynamics and control. Springer Science & Business Media; 2011.
[41] Falcone P, Tufo M, Borrelli F, Asgari J, Tseng HE. A linear time varying model predictive control approach to the integrated vehicle dynamics control problem in autonomous systems. In: 2007 46th IEEE conference on decision and control. IEEE; 2007. p. 2980–5.
[42] Bakker E, Nyborg L, Pacejka HB. Tyre modelling for use in vehicle dynamics studies. SAE Trans 1987:190–204.
[43] Liaw BY. Fuzzy logic based driving pattern recognition for driving cycle analysis. Journal of Asian Electric Vehicles 2004;2:551–6.
[44] Kim JS, Chen J, Garcia HE. Modeling, control, and dynamic performance analysis of a reverse osmosis desalination plant integrated within hybrid energy systems. Energy 2016;112:52–66.
[45] Garcia HE, Chen J, Kim JS, Vilim RB, Binder WR, Sitton SM, Boardman RD, McKellar MG, Paredis CJ. Dynamic performance analysis of two regional nuclear hybrid energy systems. Energy 2016;107:234–58.